



CHORUS

This is the accepted manuscript made available via CHORUS. The article has been published as:

Evidence of a second-order Peierls-driven metal-insulator transition in crystalline NbO₂

Matthew J. Wahila, Galo Paez, Christopher N. Singh, Anna Regoutz, Shawn Sallis, Mateusz J. Zuba, Jatinkumar Rana, M. Brooks Tellekamp, Jos E. Boschker, Toni Markurt, Jack E. N. Swallow, Leanne A. H. Jones, Tim D. Veal, Wanli Yang, Tien-Lin Lee, Fanny Rodolakis, Jerzy T. Sadowski, David Prendergast, Wei-Cheng Lee, W. Alan Doolittle, and Louis F. J. Piper

Phys. Rev. Materials **3**, 074602 — Published 16 July 2019

DOI: [10.1103/PhysRevMaterials.3.074602](https://doi.org/10.1103/PhysRevMaterials.3.074602)

Evidence of a 2nd-Order Peierls-Driven Metal-Insulator Transition in Crystalline NbO₂

Matthew J. Wahila,¹ Galo Paez,¹ Christopher N. Singh,¹ Anna Regoutz,² Shawn Sallis,³ Mateusz J. Zuba,³ Jatinkumar Rana,¹ M. Brooks Tellekamp,⁴ Jos E. Boschker,⁵ Toni Markurt,⁵ Jack E. N. Swallow,⁶ Leanne A. H. Jones,⁶ Tim D. Veal,⁶ Wanli Yang,⁷ Tien-Lin Lee,⁸ Fanny Rodolakis,⁹ Jerzy T. Sadowski,¹⁰ David Prendergast,¹¹ Wei-Cheng Lee,¹ W. Alan Doolittle,⁴ and Louis F. J. Piper^{1,3,*}

¹*Department of Physics, Binghamton University,
State University of New York, Binghamton, NY 13850, USA*

²*Department of Materials, Imperial College London, London SW7 2AZ, UK*

³*Materials Science and Engineering, Binghamton University,
State University of New York, Binghamton, NY 13850, USA*

⁴*School of Electrical and Computer Engineering,
Georgia Institute of Technology, Atlanta, GA 30332, USA*

⁵*Leibniz-Institut für Kristallzüchtung, Max-Born Strae 2, 12489 Berlin, DE*

⁶*Stephenson Institute for Renewable Energy and Department of Physics, University of Liverpool, Liverpool L69 7ZF, UK*

⁷*Advanced Light Source, Lawrence Berkeley National Laboratory, Berkeley, CA 94720, USA*

⁸*Diamond Light Source Ltd., Harwell Science and Innovation Campus, Didcot OX11 0DE, UK*

⁹*Argonne National Laboratory, 9700 South Cass Avenue, Argonne, IL 60439, USA*

¹⁰*Center for Functional Nanomaterials, Brookhaven National Laboratory, Upton, NY 11973, USA*

¹¹*The Molecular Foundry, Lawrence Berkeley National Laboratory, Berkeley, CA 94720, USA*

(Dated: June 27, 2019)

The metal-insulator transition of NbO₂ is thought to be important for the functioning of recent niobium oxide-based memristor devices, and is often described as a Mott transition in these contexts. However, the actual transition mechanism remains unclear, as current devices actually employ electroformed NbO_x that may be inherently different to crystalline NbO₂. We report on our synchrotron x-ray spectroscopy and density functional theory study of crystalline, epitaxial NbO₂ thin films grown by Pulsed Laser Deposition and Molecular Beam Epitaxy across the metal-insulator transition at ~ 810 °C. The observed spectral changes reveal a second-order Peierls transition driven by a weakening of Nb dimerization without significant electron correlations, further supported by our density functional theory modeling. Our findings indicate that employing crystalline NbO₂ as an active layer in memristor devices may facilitate analog control of the resistivity whereby Joule-heating can modulate Nb-Nb dimer distance and consequently control the opening of a pseudogap.

I. INTRODUCTION

Niobium oxide-based memristor devices have demonstrated various switching behaviors making them attractive as building blocks for neuromorphic circuits.[1–4] In the majority of reports to date, disordered Nb₂O₅ is deposited between metal electrodes and then activated using an electroforming process to reduce regions of the material to NbO_x. The switching mechanism of the activated NbO_x layer has then been explained in the literature in terms of both a Poole-Frenkel mechanism[5] and a Mott transition associated with NbO₂ nanostructures.[3, 6, 7] Without a good understanding of the true switching origin, it is difficult to further improve these devices and potentially circumvent electroforming with its associated scaling issues. It is therefore critically important to investigate the fundamental physics of the NbO_x materials used within these devices and distinguish between the different proposed mechanisms. For example, recent studies of amorphous Nb₂O₅-based devices have revealed a Poole-Frenkel conduction mechanism that enables a memdiode behavior

without utilizing any electroforming.[8]

Recent advances in the quality of pure-phase, crystalline NbO₂ films[9] could enable device architectures that directly utilize the metal-insulator transition (MIT), assumed by many to be critical to the NbO_x memristance. However, the nature of the NbO₂ MIT remains unclear and is often invoked as a Mott transition purely by comparison to VO₂, wherein a cooperative Mott-Peierls transition occurs.[10–13] Density functional theory (DFT) calculations of crystalline NbO₂ polymorphs have instead supported a Peierls mechanism, since the insulating body centered tetragonal (BCT) and metallic rutile phases can both be reproduced without requiring electron-correlation effects to open and close a band gap.[14, 15] This has been further supported by recent DFT combined with the slave spin method (DFT+SS).[16] DFT+SS is capable of describing a strain-induced orbital selective Mott transition observed in VO₂, which is seemingly not possible in NbO₂. However, any attempts at direct comparison between these calculations and experimental x-ray spectroscopy results have suffered due to material issues associated with the surface-sensitive techniques employed[17] and the high MIT temperature ($T_c = 1083$ K) of NbO₂. [18]

Here, we report on our temperature-dependent synchrotron spectroscopy studies of crystalline NbO₂ films

* lpiper@binghamton.edu

probing the true nature of the MIT. We employ hard x-ray photoelectron spectroscopy (HAXPES) and fluorescent yield x-ray absorption spectroscopy (XAS) to circumvent surface issues and fingerprint the bulk insulating and metallic phases of NbO₂. DFT calculations and many body simulations of the valence and conduction band spectra, respectively, are compared to the experimental spectra and reinforce that the band gap is formed mainly by Nb-Nb dimer formation. Variable photon energy and temperature-dependent soft x-ray photoelectron spectroscopy (XPS) are then used to characterize the film surface and distinguish between the surface and bulk band evolution occurring across the MIT. Finally, EXAFS fitting is used to confirm the temperature response of Nb dimers within the bulk insulating phase.

We report on the high temperature stability of NbO₂, which displays little to no bulk oxygen loss even after heating to 1600 °C. And we confirm the existence of an intrinsic and atomically-thin Nb⁵⁺ surface reconstruction that does not participate in the bulk dimerization. Our analysis reveals that bulk NbO₂ undergoes a gradual temperature-dependent evolution of states at the Fermi level, which can be modeled in terms of a pseudogap that gradually opens with decreasing Nb-Nb dimer distance (i.e., a second-order Peierls-driven MIT). These results indicate that Mott physics does not play a significant role in the transition of crystalline NbO₂, with only weak contributions possible from any electron correlations due to the wide Nb 4d orbital bandwidth. Our work clarifies the true nature of the MIT in crystalline NbO₂ as Peierls-driven and reveals the importance of Nb dimer distance to the electronic conductivity.

II. METHODS

Crystalline NbO₂ films were grown using both pulsed laser deposition (PLD) and molecular beam epitaxy (MBE). Approximately 400 nm thick, (440)-oriented NbO₂ films were grown epitaxially on 430 μm thick, 10 × 10 mm, single crystalline, c-plane (006)-oriented Al₂O₃ substrates using a Varian Gen-II style MBE system at the Georgia Institute of Technology. Prior to deposition, substrates were cleaned with acetone, methanol, and isopropyl alcohol followed by a 4:1 H₂SO₄:H₂O₂ wash at 120 °C. Substrates were then loaded and degassed in a separate chamber, with care taken during loading to minimize sample contact with the surrounding metal substrate holder which will conduct thermal energy away from the sample creating thermal non-uniformity. Thin films were then grown under a 4 SCCM O₂ flow at high temperatures (950 - 1000 °C). It should be noted that higher temperatures than typically used in MBE were necessary to achieve high quality NbO₂ films. Additional growth details have been previously reported.[9]

In addition, (100)-oriented NbO₂ films were grown on single crystalline, (110)-oriented TiO₂ substrates using a PLD system at the Leibniz-Institut für Kristallzüchtung.

Prior to deposition, substrates were annealed for 2 hours at 1000 °C in an oxygen atmosphere. The thin films were subsequently deposited via PLD using a KrF excimer laser operated at 1 Hz to ablate a NbO₂ target with a 60 mm substrate to target distance. Depositions were carried out under a 0.1 mbar Ar atmosphere with a 650 °C substrate temperature. Depositions were monitored using in-situ RHEED. The fluency was 2.1/2.5 J/cm² and 3000/20000 pulses were used for each deposition resulting in films with a thickness of approximately 18 nm/111 nm, as determined from the thickness fringes around the NbO₂ (400) diffraction peak.

Hard x-ray photoelectron spectroscopy (HAXPES) was performed with a 5932 eV photon energy at the I09 beamline of the Diamond Light Source (DLS) in Oxfordshire, UK. Spectra were energy-resolved and measured using a VG Scienta EW4000 high-energy electron-energy analyzer with a ± 30° acceptance angle. The photon beam was monochromated using a Si(111) double-crystal monochromator followed by a channel cut Si(004) crystal, resulting in an energy resolution of < 250 meV.[19–21]

Variable photon energy x-ray photoelectron spectroscopy (XPS) was performed at beamline 29-ID of the Advanced Photon Source (APS) at Argonne National Laboratory in Lemont, IL. Temperature-dependent x-ray photoelectron spectroscopy (T-XPS) was performed at the Electron Spectro-Microscopy (ESM) beamline 21-ID of the National Synchrotron Light Source-II at Brookhaven National Laboratory in Upton, NY.

O K-edge x-ray absorption spectroscopy (XAS) was performed at beamline 8 of the Advanced Light Source (ALS) in Berkeley, CA. Spectra were taken in both total electron yield (TEY) and total fluorescence mode (TFY), with an effective resolution of ~ 200 meV. Spectra were normalized to the current from an Au-coated reference mesh in the path of the incident photon beam. Energy calibration was performed using the first- and second-order diffraction Ti L_{3,2}-edge and O K-edge absorption features of a rutile TiO₂ reference.

Temperature-dependent Nb K-edge extended x-ray absorption fine structure (EXAFS) measurements were performed on commercially produced NbO₂ powder (CAS Number 12034-59-2) at beamline 20-BM of the APS. Measurements were performed only up to 400 °C, as oxidation to Nb⁵⁺ was found to occur when annealing at atmospheric pressures, even when using an inert gas flow to reduce oxygen exposure. Energy calibration was performed by energy shifting the maximum of the first peak in the derivative spectrum of a pure Nb reference foil to the Nb K-edge reference energy (18986 eV). Data processing was carried out using the ATHENA software from the IFEFFIT package.[22, 23] The undulatory region of the normalized spectrum was first converted into k-space. The resultant χ(k) was then k²-weighted to enhance higher k in the Fourier transformation of k²χ(k), thus enabling model peak fitting. To resolve the Nb-Nb dimer peak and inter-atomic length precisely, a theoretical model spectrum was generated

via ab-initio calculations with relevant structural data using the FEFF8.2 code[24] and then least-square fit to the data using ARTEMIS.

Density functional theory (DFT) calculations were performed within the WIEN2k[25] ecosystem employing full potential linear augmented plane waves plus local orbitals (FP-LAPW+lo) and the generalized gradient approximation of Purdue-Burke-Erzenhof (PBE).[26] The total energy was converged to 0.1 meV on a 1000 k-point grid with an RKmax of 6.5. Ionic relaxations were performed with VASP[27, 28] with a cutoff energy of 750 eV on an $8 \times 8 \times 12$ and $8 \times 8 \times 8$ k-mesh for rutile and BCT phases. Many body x-ray absorption simulations were performed to using a constrained-occupancy delta-self-consistent-field approach rectified by explicitly calculating many-electron transition amplitudes, as described by Prendergast et al.[29]

III. RESULTS

NbO_2 is known to undergo a transition between an insulating BCT phase containing Nb dimers and a more symmetric, metallic rutile phase around ~ 810 °C, both depicted in Figure 1 (a). HAXPES valence band spectra and fluorescent yield XAS O K-edge spectra, shown in Figure 1 (b) and (c) respectively, reflect the density of occupied valence states and partial density of unoccupied O 2p conduction states in the low and high temperature phases of crystalline $\text{NbO}_2/\text{TiO}_2$. Corresponding Nb 3d core-level HAXPES confirms a Nb^{4+} oxidation state in the bulk of the film (refer to supplemental information). The increased probing depth afforded by these high photon energy methods reduces the spectral contamination from Nb^{5+} surface components observed in other studies,[17] as discussed further below.

The valence band spectra display the occupied Nb 4d t_{2g} state clearly separated from the main O 2p-derived valence band and centered ~ 1 eV below the Fermi level in the insulating phase, in agreement with DFT calculations. Consistent with previous reports of weak electron correlation effects, the band theory calculations are sufficient to accurately reproduce a band opening without the need for +U corrections, although they underestimate the band gap magnitude.[14–17] Unfortunately, the small band gap of the low temperature BCT phase means the O K-edge XAS cannot be compared to the unoccupied O 2p partial density of states calculated using DFT. To account for the many-body dynamic excitations occurring due to NbO_2 being a near-metallic oxide, we employed a self-consistent-field approach by Prendergast et al.[29] The simulated absorption for the dimerized BCT phase is found to agree well with the low temperature experimental data. Taken together, these results are consistent with the insulating phase arising from mainly Nb dimerization (Peierls) rather than electron correlation (Mott).

To investigate the electronic evolution of NbO_2 across the MIT, surface sensitive XPS was performed on

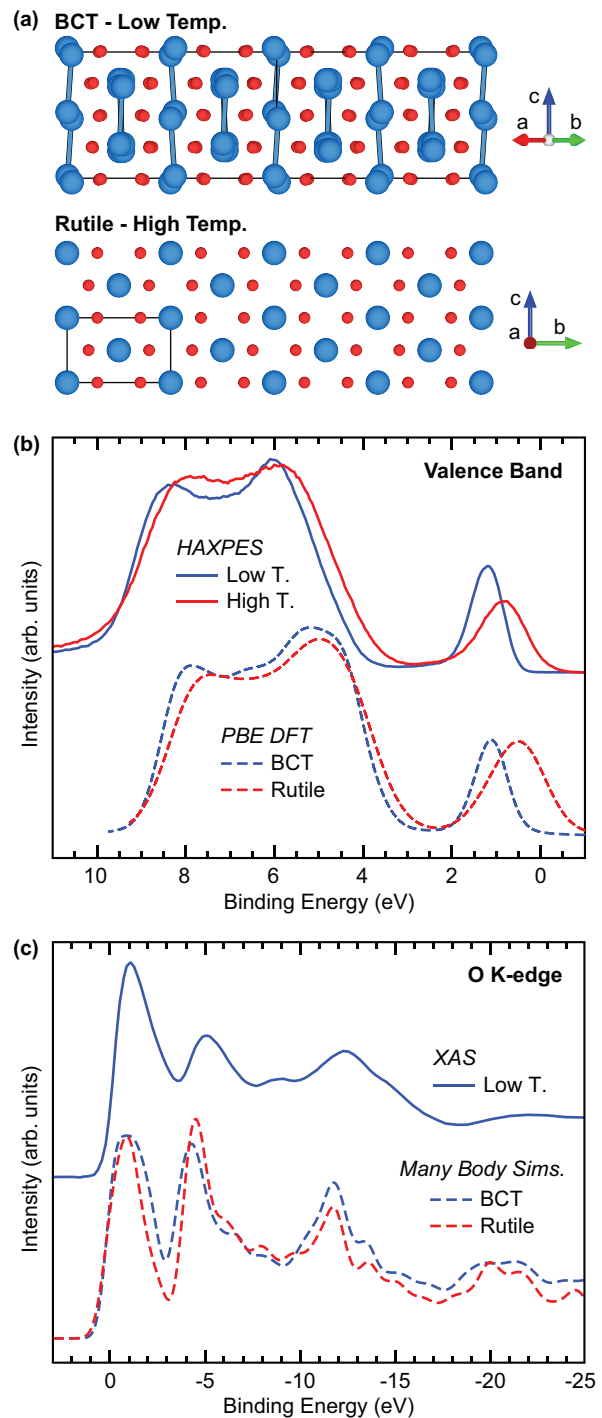


FIG. 1. (a) Low temperature BCT and high temperature rutile crystal structures of NbO_2 . (b) Valence band and (c) oxygen k-edge spectra, both measured and calculated, for the low temperature BCT (blue) and high temperature rutile (red) phases of a crystalline $\text{NbO}_2/\text{TiO}_2$ thin film.

$\text{NbO}_2/\text{Al}_2\text{O}_3$ at several soft x-ray synchrotron beamlines. To remove surface contaminants and reduce any over-oxidation of the films arising from atmospheric exposure that might complicate results from these surface sensitive

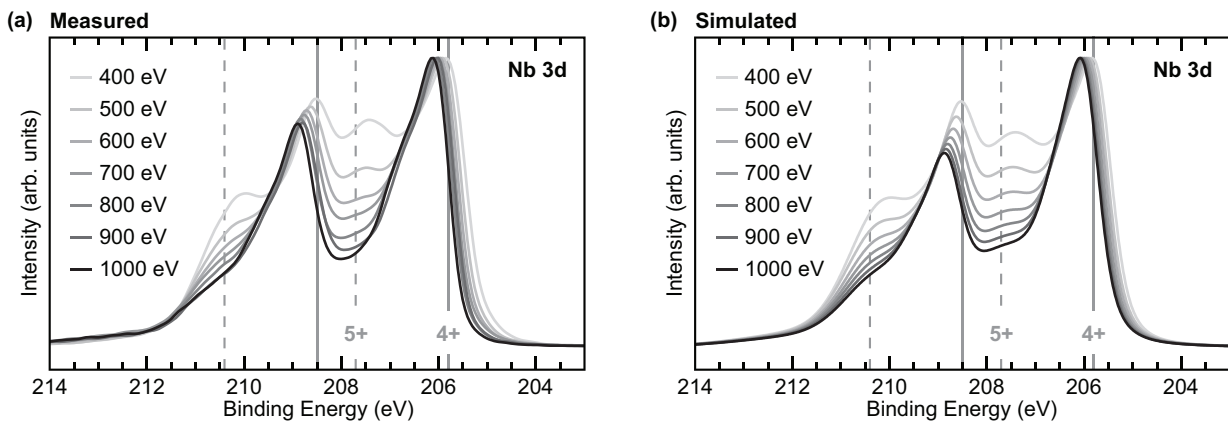


FIG. 2. (a) Variable photon energy XPS of the Nb 3d region for $\text{NbO}_2/\text{Al}_2\text{O}_3$ at room temperature, and (b) simulated spectra assuming a 0.9 nm Nb_2O_5 (Nb^{5+}) surface layer on top of the NbO_2 (Nb^{4+}) bulk. Approximate Nb^{4+} and Nb^{5+} spin-split peak energies are identified.

techniques, clean and well-ordered sample surfaces were achieved by annealing the films in vacuo at high temperatures near and above the MIT. Sapphire substrates were used here as the TiO_2 substrate used for the previous HAXPES experiments proved to be too unstable at high temperatures, resulting in oxygen migration from the substrate and into the NbO_2 film. After preparation, the sample surfaces were thoroughly characterized before investigating the MIT behavior to ensure that any results are properly attributed to either bulk or surface effects.

Figure 2 (a) displays non-destructive depth profiling of the $\text{NbO}_2/\text{Al}_2\text{O}_3$ performed using Nb 3d core-level spectra measured at multiple incident x-ray photon energies. The spectra reveal both Nb^{4+} and Nb^{5+} oxidation states existing within the film. However, the lower the incident photon energy (i.e., the more surface sensitive the measurement), the more enhanced the Nb^{5+} peaks become relative to the Nb^{4+} , indicating the Nb^{5+} is restricted to the very topmost surface layer. Shown in Figure 2 (b), simulated XPS spectra were created by modeling the film as a two layer system with a Nb_2O_5 (Nb^{5+}) surface layer on top of an NbO_2 (Nb^{4+}) bulk film (refer to supplemental information). A Nb_2O_5 surface layer thickness of 0.9 nm is found to result in good agreement with the experimentally observed trend. This confirms that the Nb^{5+} is restricted to only the topmost atomic layers (~ 1 nm) of the NbO_2 film.

Further supporting this conclusion, only a slight reduction in the amount of surface Nb^{5+} was observed after annealing above the MIT temperature for the first time (refer to supplemental information). And no amount of further annealing up to 1600° removed the remaining Nb^{5+} surface layer, nor did it reduce the bulk Nb^{4+} , as confirmed by HAXPES (refer to supplemental information). The robust nature of NbO_2 regarding oxygen loss at high temperatures is note-worthy given the potential role of Joule-heating in the switching of NbO_x -based devices. This data suggests that our $\text{NbO}_2/\text{Al}_2\text{O}_3$ film has a strong proclivity towards forming an inert Nb^{5+} sur-

face, likely the result of a preferred surface termination rather than an over-oxidation of the film. This inert surface must be accounted for when using highly surface sensitive techniques like XPS, LEED, or LEEM/PEEM to investigate the MIT behavior.

Figure 3 shows temperature-dependent XPS of the O 1s, Nb 3d, and valence band regions of the $\text{NbO}_2/\text{Al}_2\text{O}_3$. The spectra were taken in descending order (starting at 1000°C and then cooling down in steps until room temperature) in order to rule out surface composition/oxidation changes due to in vacuo heating as the cause of increased metallicity at high temperatures. In addition, these temperature-dependent measurements were repeated multiple times to fully ensure the spectral changes reported herein are reversible and not due to irreversible sample damage such as oxygen loss (refer to supplemental information).

The transition between metallic and insulating states is readily apparent from changes near the Fermi level. Spectral weight is found to shift towards the Fermi level with increasing temperature, causing the eventual closure of the band gap at the MIT temperature. This transition is gradual, occurring over a wide range of several hundred degrees, rather than abruptly as would be expected for a first-order transition like in VO_2 .^[30] This observation is consistent with previous temperature-dependent conductivity studies of NbO_2 crystals,^[18] where an almost 9 orders of magnitude change in conductivity was found to gradually occur over a wide temperature range below the official MIT temperature. It must be noted that while the films display both Nb^{5+} 'surface' and NbO_2 'bulk' signal contributions due to the surface sensitivity of the XPS, the Nb^{5+} surface does not contribute any spectral weight to the occupied Nb 4d states at the Fermi level responsible for the change in metallicity.

As the NbO_2 is heated towards the transition temperature, two different effects are observed in the XPS spectra which must be disentangled to understand the MIT. There is a symmetric thermal broadening affect-

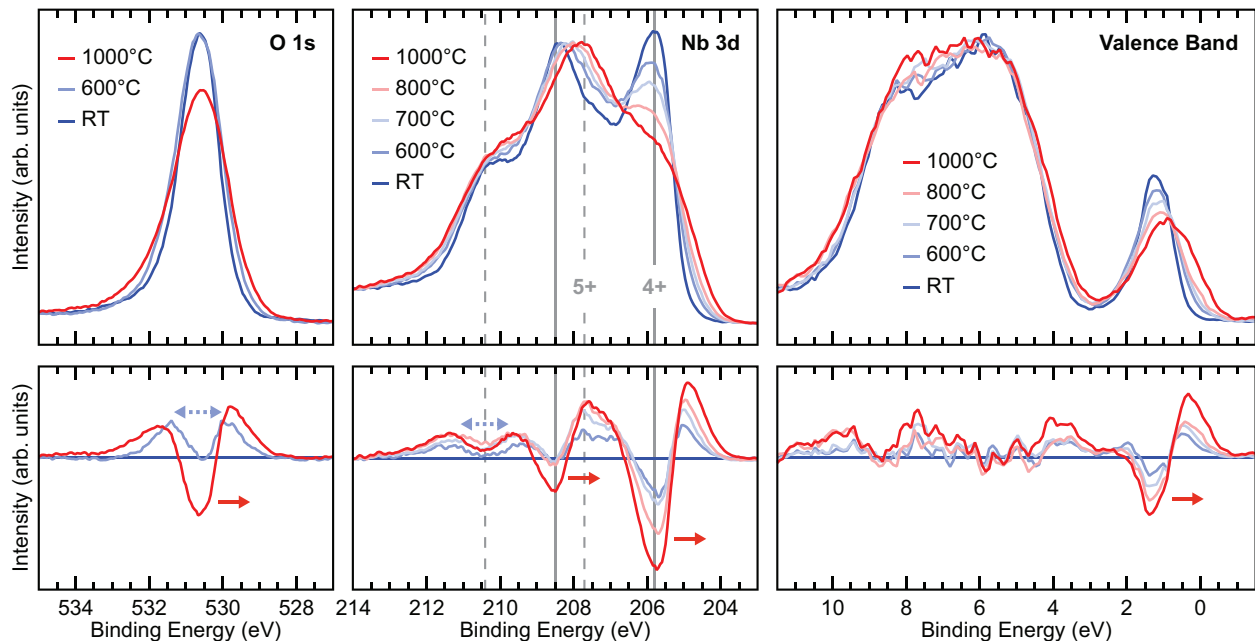


FIG. 3. (top) Temperature-dependent XPS of the O 1s region ($h\nu = 700$ eV), and the Nb 3d and valence band regions ($h\nu = 450$ eV) of NbO₂/Al₂O₃. Nb 3d peak positions for Nb⁵⁺ and Nb⁴⁺ charge states are denoted. (bottom) Difference spectra showing the spectral changes in the O 1s, Nb 3d, and valence band regions relative to the room temperature measurements. Red solid arrows indicate asymmetric broadening, while blue dashed arrows indicate symmetric broadening.

ing all spectral features and an asymmetric broadening to lower binding energies only affecting certain spectral features. These effects are more readily distinguished in the difference spectra plotted below the XPS, which use the room temperature XPS spectra as an internal reference. The symmetric broadening (blue dashed arrows) is most easily observed in the Nb⁵⁺ contributions of the Nb 3d region. Meanwhile, the asymmetric broadening (red solid arrows) is clearly observed in the Nb⁴⁺-related states. The asymmetric broadening is consistent with a modulation of final state screening effects associated with the formation of states at the Fermi level (i.e., an increase in metallicity). The O 1s region further supports this, displaying only symmetric thermal broadening up to the MIT temperature, at which point an asymmetric broadening abruptly appears. Similar O 1s evolution is observed across the MIT of other metal oxides.[31] As mentioned previously, the transition is reversible with the NbO₂ fully recovering to its initial state upon cooling.

Figure 4 (a) plots the DFT quasiparticle density of states near the Fermi level for NbO₂ as the Nb dimer length varies between that of the fully dimerized BCT phase and the non-dimerized rutile phase. For the electronic structure simulations, the high and low temperature phases were both represented in a single ($I4_1/a88$) body centered tetragonal space group.[17] Using a common lattice was necessary to interpolate the structural phases between the experimentally determined rutile and BCT endpoints. Connecting the two phases was then achieved by linearly interpolating the Nb-Nb bond lengths along the dimerization axis (*c*-axis).

As the Nb dimers form (Nb-Nb bond length decreases), there is a concomitant increase in electron localization. This gradually increasing localization results in the formation of a pseudogap that eventually opens into a full band gap, creating a fully insulating phase.[14, 15, 17] This is in contrast to the action of a Hubbard *U* correction, which does not gap the spectrum in the metallic phase, nor does it act to significantly change the electronic character in the insulating phase (refer to supplemental information). This shows that the number of occupied states at the chemical potential is highly sensitive to lattice deformations, and only weakly governed by electronic correlations. However, it is not just the form of the quasiparticle density of states that suggests a strong Peierls mechanism, but also the excellent agreement observed between the hard/soft x-ray spectral features and the calculations performed at the PBE level. These results indicate that electron-electron contributions to the ground state energy must be small compared to contributions from the lattice degrees of freedom.

Temperature-dependent EXAFS fitting results, shown in Figure 4 (b), also support the idea of a Nb dimer weakening with increased temperature. As temperature increases, the average Nb-Nb dimer length is found to increase in a manner that coincides with the predicted opening of a pseudogap, as calculated using both PBE DFT and the generalized solid-state nudged elastic band (G-SSNEB) method.[14] This experimental confirmation of a gradual structural transition reinforces the idea of a second-order mechanism relating to Nb dimerization. Combining this with the previously described confirma-

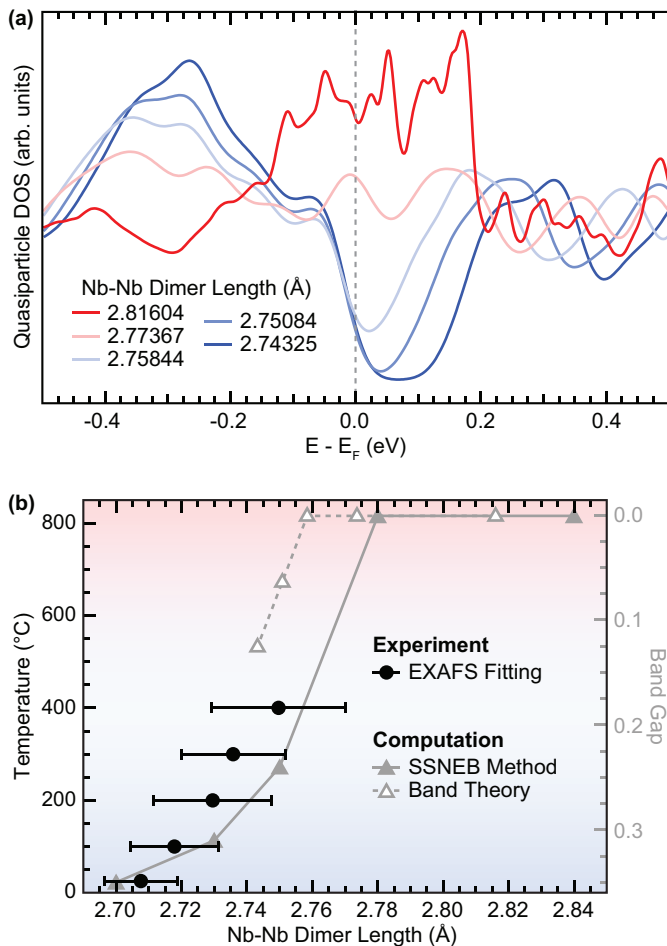


FIG. 4. (a) PBE DFT calculated density of states at the Fermi level for crystalline NbO_2 with increasing Nb dimer distance. (b) Temperature-dependent EXAFS fitting results of the Nb dimer distance (left axis) compared to DFT and SSNEB[14] calculated bandgaps (right axis).

tion of a gradual electronic transition and the lack of any observed electron correlation effects, we conclude that the MIT behavior of NbO_2 is best described in terms of a second-order, temperature-dependent Peierls transition, rather than a Mott transition.

IV. CONCLUSION

Crystalline NbO_2 is conclusively found to undergo a second-order, temperature-dependent Peierls transition with little to no contribution from electron correlations. Our results indicate that as the temperature within crystalline NbO_2 is increased by local Joule-heating, an insulator-to-metal phase transformation would likely occur due to a weakening of local Nb-Nb dimers, resulting

in memristor-like switching. Moreover, our results imply that the use of crystalline NbO_2 as the active layer in next-generation memristive components has two major benefits. Firstly, an electroforming step would not be required to induce the MIT-based switching behavior, making it more appealing for industrial scale employment. Secondly, precise control of local Joule-heating is expected to enable analog modulation of the resistive state, due to the analog temperature-sensitivity of the Nb-Nb dimer length within the BCT phase. In addition, although strain-engineering epitaxial NbO_2 films is not expected to increase electron correlation effects because of the Nb 4d bandwidth, it could potentially be employed as a method to tune Nb-Nb dimer distance for further control of resistive states.

V. ACKNOWLEDGMENTS

We would like to thank Prof. David Scanlon and Dr. Alex Ganose from University College London for fruitful discussions regarding the atomistic calculations. This material is based upon work supported by the Air Force Office of Scientific Research under award No. FA9550-18-1-0024. Anna Regoutz acknowledges the support from Imperial College London for her Imperial College Research Fellowship. Jack E. N. Swallow acknowledges studentship support from the EPSRC Centre for Doctoral Training in New and Sustainable Photovoltaics (Grant No. EP/L01551X/1). Leanne A. H. Jones's studentship was funded by the EPSRC Doctoral Training Partnership (Grant No. EP/R513271/1). Jos E. Boschker acknowledges support from the Leibniz association within the Leibniz Competition through a project entitled Physics and control of defects in oxide films for adaptive electronics. This work was supported by the Engineering and Physical Sciences Research Council (EPSRC) (Grant Nos. EP/N015800/1). We acknowledge Diamond Light Source for time on Beamline I09 under Proposals SI20647 and SI21430. This research used resources of the Center for Functional Nanomaterials and the National Synchrotron Light Source II, which are U.S. Department of Energy (DOE) Office of Science facilities at Brookhaven National Laboratory, under Contract No. DE-SC0012704. This research used resources of the Advanced Light Source and the Molecular Foundry, which are U.S. DOE Office of Science facilities at Lawrence Berkeley National Laboratory under Contract No. DE-AC02-05CH11231. This research used resources of the Advanced Photon Source, a U.S. DOE Office of Science User Facility operated for the DOE Office of Science by Argonne National Laboratory under Contract No. DE-AC02-06CH11357; additional support by National Science Foundation under Grant no. DMR-0703406.

[1] S. Kumar, J. P. Strachan, and R. S. Williams, *Nature* **548**, 318 (2017).

[2] L. Gao, P.-Y. Chen, and S. Yu, *Applied Physics Letters* **111**, 103503 (2017),

- <https://doi.org/10.1063/1.4991917>.
- [3] M. D. Pickett, G. Medeiros-Ribeiro, and R. S. Williams, *Nature Materials* **12**, 114 (2012).
- [4] Y. Zhou and S. Ramanathan, *Proceedings of the IEEE* **103**, 1289 (2015).
- [5] Z. Wang, S. Kumar, Y. Nishi, and H.-S. P. Wong, *Applied Physics Letters* **112**, 193503 (2018), <https://doi.org/10.1063/1.5027152>.
- [6] M. D. Pickett and R. S. Williams, *Nanotechnology* **23**, 215202 (2012).
- [7] S. Kumar, Z. Wang, N. Davila, N. Kumari, K. J. Norris, X. Huang, J. P. Strachan, D. Vine, A. L. D. Kilcoyne, Y. Nishi, and R. S. Williams, *Nature Communications* **8**, 658 (2017).
- [8] J. C. Shank, M. B. Tellekamp, M. J. Wahila, S. Howard, A. S. Weidenbach, B. Zivasatienraj, L. F. J. Piper, and W. A. Doolittle, *Scientific Reports* **8**, 12935 (2018).
- [9] M. B. Tellekamp, J. C. Shank, and W. A. Doolittle, *Journal of Crystal Growth* **463**, 156 (2017).
- [10] M. W. Haverkort, Z. Hu, A. Tanaka, W. Reichelt, S. V. Streltsov, M. A. Korotin, V. I. Anisimov, H. H. Hsieh, H.-J. Lin, C. T. Chen, D. I. Khomskii, and L. H. Tjeng, *Phys. Rev. Lett.* **95**, 196404 (2005).
- [11] T. C. Koethe, Z. Hu, M. W. Haverkort, C. Schüßler-Langeheine, F. Venturini, N. B. Brookes, O. Tjernberg, W. Reichelt, H. H. Hsieh, H.-J. Lin, C. T. Chen, and L. H. Tjeng, *Phys. Rev. Lett.* **97**, 116402 (2006).
- [12] N. F. Quackenbush, H. Paik, M. E. Holtz, M. J. Wahila, J. A. Moyer, S. Barthel, T. O. Wehling, D. A. Arena, J. C. Woicik, D. A. Muller, D. G. Schlom, and L. F. J. Piper, *Phys. Rev. B* **96**, 081103(R) (2017).
- [13] S. Mukherjee, N. F. Quackenbush, H. Paik, C. Schlueter, T.-L. Lee, D. G. Schlom, L. F. J. Piper, and W.-C. Lee, *Phys. Rev. B* **93**, 241110(R) (2016).
- [14] A. O'Hara and A. A. Demkov, *Phys. Rev. B* **91**, 094305 (2015).
- [15] V. Eyert, *EPL (Europhysics Letters)* **58**, 851 (2002).
- [16] W. C. Lee, M. J. Wahila, S. Mukherjee, C. N. Singh, T. Eustance, A. Regoutz, H. Paik, J. E. Boschker, F. Rodolakis, T. L. Lee, D. G. Schlom, and L. F. Piper, *Journal of Applied Physics* **125** (2019), [10.1063/1.5052636](https://doi.org/10.1063/1.5052636).
- [17] A. O'Hara, T. N. Nunley, A. B. Posadas, S. Zollner, and A. A. Demkov, *Journal of Applied Physics* **116**, 213705 (2014), <https://doi.org/10.1063/1.4903067>.
- [18] Y. Sakai, N. Tsuda, and T. Sakata, *Journal of the Physical Society of Japan* **54**, 1514 (1985).
- [19] J. Kelly and S. G. Alcock, *Journal of Physics: Conference Series* **425**, 052024 (2013).
- [20] L. W. Wangoh, S. Sallis, K. M. Wiaderek, Y.-C. Lin, B. Wen, N. F. Quackenbush, N. A. Chernova, J. Guo, L. Ma, T. Wu, T.-L. Lee, C. Schlueter, S. P. Ong, K. W. Chapman, M. S. Whittingham, and L. F. J. Piper, *Applied Physics Letters* **109**, 053904 (2016).
- [21] N. F. Quackenbush, H. Paik, M. J. Wahila, S. Sallis, M. E. Holtz, X. Huang, A. Ganose, B. J. Morgan, D. O. Scanlon, Y. Gu, F. Xue, L. Q. Chen, G. E. Sterbinsky, C. Schlueter, T. L. Lee, J. C. Woicik, J. H. Guo, J. D. Brock, D. A. Muller, D. A. Arena, D. G. Schlom, and L. F. J. Piper, *Phys. Rev. B* **94**, 085105 (2016).
- [22] M. Newville, *Journal of synchrotron radiation* **8**, 322 (2001).
- [23] B. Ravel and M. Newville, *Journal of synchrotron radiation* **12**, 537 (2005).
- [24] A. L. Ankudinov, B. Ravel, J. J. Rehr, and S. D. Conradson, *Physical Review B* **58**, 7565 (1998).
- [25] P. Blaha, K. Schwarz, G. K. H. Madsen, D. Kvasnicka, and J. Luitz, *WIEN2K, An Augmented Plane Wave + Local Orbitals Program for Calculating Crystal Properties* (Karlheinz Schwarz, Techn. Universität Wien, Austria, 2001).
- [26] J. P. Perdew, K. Burke, and M. Ernzerhof, *Phys. Rev. Lett.* **77**, 3865 (1996).
- [27] G. Kresse and J. Furthmüller, *Phys. Rev. B* **54**, 11169 (1996).
- [28] G. Kresse and J. Furthmüller, *Computational Materials Science* **6**, 15 (1996).
- [29] Y. Liang, J. Vinson, S. Pemmaraju, W. S. Drisdell, E. L. Shirley, and D. Prendergast, *Phys. Rev. Lett.* **118**, 096402 (2017).
- [30] W. H. Brito, M. C. O. Aguiar, K. Haule, and G. Kotliar, *Phys. Rev. B* **96**, 195102 (2017).
- [31] N. F. Quackenbush, J. W. Tashman, J. A. Mundy, S. Sallis, H. Paik, R. Misra, J. A. Moyer, J.-H. Guo, D. A. Fischer, J. C. Woicik, D. A. Muller, D. G. Schlom, and L. F. J. Piper, *Nano Letters* **13**, 4857 (2013).